European Radiology (2019) 29:6089–6099
https://doi.org/10.1007/s00330-019-06235-3

CHEST

Differential diagnosis of pulmonary infections in immunocompromised patients using high-resolution computed tomography

Yoshie Kunihiro[1,2] · Nobuyuki Tanaka[1,2] · Reo Kawano[3] · Toshiaki Yujiri[4] · Makoto Kubo[5] · Kazuhiro Ueda[6] · Toshikazu Gondo[7] · Taiga Kobayashi[2] · Tsuneo Matsumoto[1]

Received: 9 October 2018 / Revised: 28 March 2019 / Accepted: 10 April 2019 / Published online: 6 May 2019

Abstract

Objectives The aims of this study were to compare the high-resolution computed tomography (HRCT) findings of pulmonary infections in immunocompromised patients and to assess the usefulness of HRCT in the differential diagnosis of these infections.

Methods A total of 345 immunocompromised patients with pulmonary infections were included in this study. The diagnoses of the patients consisted of bacterial pneumonia (123 cases), pneumocystis pneumonia (PCP) (105 cases), fungal pneumonia (80 cases), tuberculosis (15 cases), cytomegalovirus pneumonia (11 cases), and septic embolism (11 cases). Two chest radiologists retrospectively evaluated the computed tomography (CT) images, which consisted of 22 findings including ground-glass attenuation, consolidation, nodules, and thickening of the bronchial wall and interlobular septum. Associations between the CT criteria and infections were investigated using χ^2 test; multiple logistic regression analyses were conducted to identify the significant indicator for each infection. The area under the curve (AUC) of each model was calculated.

Results Bronchial wall thickening was a significant indicator for bacterial pneumonia ($p = 0.002$; odds ratio [OR], 2.341; 95% confidence interval [CI], 1.378–3.978). The presence of a mosaic pattern and the absence of nodules were significant indicators for PCP ($p < 0.001$; OR, 9.808; 95% CI, 4.883–13.699, and $p < 0.001$; OR, 6.834; 95% CI, 3.438–13.587, respectively). The presence of nodules was a significant indicator for fungal infection ($p = 0.005$; OR, 2.531; 95% CI, 1.326–4.828). The AUC for PCP was the highest (0.904).

Conclusions HRCT findings are potentially useful for the differential diagnosis of some pulmonary infections in immunocompromised patients.

Key Points

- *Differential diagnosis of pulmonary infections in immunocompromised patients could be established with the help of high-resolution computed tomography.*
- *Bronchial wall thickening was a significant indicator for bacterial pneumonia.*
- *The presence of a mosaic pattern and the absence of nodules were significant indicators for pneumocystis pneumonia.*

Keywords X-ray computed tomography · Pneumonia · Immunocompromised host · Multivariate analysis

✉ Yoshie Kunihiro
kyoshie@yamaguchi-u.ac.jp

[1] Department of Radiology, National Hospital Organization Yamaguchi - Ube Medical Center, 685 Higashikiwa, Ube, Yamaguchi 755-0241, Japan

[2] Department of Radiology, Yamaguchi University Graduate School of Medicine, 1-1-1 Minamikogushi, Ube, Yamaguchi 755-8505, Japan

[3] Center for Integrated Medical Research, Hiroshima University Hospital, Kasumi 1-2-3 Minami-ku, Hiroshima, Hiroshima 734-8551, Japan

[4] Division of Endocrinology, Metabolism, Hematological Science and Therapeutics, Yamaguchi University Graduate School of Medicine, 1-1-1 Minamikogushi, Ube, Yamaguchi 755-8505, Japan

[5] Department of Medicine and Clinical Science, Yamaguchi University Graduate School of Medicine, 1-1-1 Minamikogushi, Ube, Yamaguchi 755-8505, Japan

[6] Department of Surgery and Clinical Science, Yamaguchi University Graduate School of Medicine, 1-1-1 Minamikogushi, Ube, Yamaguchi 755-8505, Japan

[7] Division of Pathology, Fujisawa City Hospital, 2-6-1 Fujisawa, Fujisawa, Kanagawa 251-8550, Japan

Abbreviations

κ	Kappa value
χ^2	Chi-square
AIDS	Acquired immunodeficiency syndrome
AUC	Area under the curve
BAL	Bronchoalveolar lavage
CI	Confidence interval
CMV-P	Cytomegalovirus pneumonia
Cons	Consolidation
CT	Computed tomography
GGA	Ground-glass attenuation
HRCT	High-resolution computed tomography
HSCT	Hematopoietic stem cell transplantation
ICC	Intraclass correlation coefficient
ILS	Interlobular septum
LN	Lymph node
NPV	Negative predictive value
OR	Odds ratio
PACS	Picture archiving and communication system
PCP	Pneumocystis pneumonia
PPV	Positive predictive value
S. aureus	*Staphylococcus aureus*
SLB	Surgical lung biopsy
TB	Tuberculosis
TBLB	Transbronchial lung biopsy
TIB	Tree-in-bud

Introduction

The number of immunocompromised patients has increased due to the advances in chemotherapy for malignant diseases and immunosuppressive therapy for autoimmune diseases and an increase in hematopoietic stem cell transplantation and solid organ transplantation. Pulmonary infection is a major cause of morbidity and mortality in immunocompromised patients.

Hospital-acquired bacterial pneumonia occurs commonly due to *Staphylococcus aureus* (*S. aureus*), *Pseudomonas aeruginosa*, and *Klebsiella pneumoniae*. Pulmonary nocardiosis is one of the important infections in immunocompromised patients [1]. Pneumocystis pneumonia (PCP) is one of the most frequent pulmonary infections in immunocompromised patients including those with human immunodeficiency virus infection [2]. The major risk factors for invasive aspergillosis include neutropenia and prolonged corticosteroid therapy. Infections by *Candida* species and *Cryptococcus neoformans* as well as mucormycosis may also occur as opportunistic infections. Cytomegalovirus pneumonia (CMV-P) is one of the major complications in transplant recipients [3]. The risk of active tuberculosis (TB) in transplant recipients is 30–50 times higher than that in the general population [4]. Although septic embolism occurs most commonly in association with right-sided endocarditis, infected indwelling catheters, intravenous drug use, and septic thrombophlebitis [5–7] can predispose to septic embolism in immunocompromised patients. The clinical presentation of pulmonary infections is nonspecific, which includes symptoms such as fever, dyspnea, and cough. Since the therapeutic strategies are different for these infectious diseases, it is important to establish an accurate diagnosis. However, the process of differential diagnosis of these infectious diseases could be quite challenging.

Imaging is essential for the diagnosis of pulmonary infections. Chest radiography is used as a screening diagnostic tool; however, it has limited sensitivity and shows normal results in up to 10% of patients with pulmonary diseases [8, 9]. Furthermore, the chest radiographic findings are often nonspecific [10]. High-resolution computed tomography (HRCT) is much more sensitive and specific than chest radiography [4]. Heussel et al reported that HRCT could detect pneumonia about 5 days earlier than that by chest radiography, and during the first 7 days, the number of pneumonias detected with HRCT was six times greater than the number detected with chest radiography [11]. In order to utilize computed tomography (CT) more frequently than chest radiography for immunocompromised patients, some institutions had explored the use of low or ultralow dose CT imaging [12].

The frequent findings in the HRCT images of pulmonary infections include nodules, tree-in-bud appearance, ground-glass attenuation (GGA), consolidation, or a combination of these findings [13–15]. The HRCT findings in pulmonary infections could be overlapping and nonspecific. There have been many HRCT imaging findings reported for pulmonary infections; however, specific findings for each infection would be necessary for establishing an early, accurate diagnosis, especially in immunocompromised patients.

The aims of this study were to compare the HRCT findings of various pulmonary infections in immunocompromised patients and to assess the usefulness of HRCT in the differential diagnosis of these infections.

Materials and methods

The institutional review board of our hospital approved this study. The requirement for informed consent was waived for this study owing to the retrospective study design.

Patients

We retrospectively reviewed the CT database at our institution for acute chest complications in immunocompromised patients from January 1990 to December 2015. The patients included in the study were those who (1) had undergone HRCT scans, (2) had HRCT findings showing parenchymal abnormalities, and (3) were diagnosed with only a single

infectious disease. At first, we identified a total of 1073 cases. Among these, 476 cases were excluded because either their lung disease could not be specified or they had pulmonary or bronchial abnormalities, such as interstitial pneumonia, radiation pneumonitis, lung cancer, severe emphysema, bronchial asthma, and graft versus host disease, which might have confounded evaluation of their HRCT findings. Among the patients suspected of fungal pulmonary infections, two were excluded due to *Aspergillus* otomycosis and *Candida* esophagitis. Among the remaining, 381 cases with pulmonary infections were identified. Specific pulmonary infections were diagnosed by detailed evaluations of the medical records and the results of one more of the most appropriate laboratory tests for each individual, including sputum culture, serologic tests for likely pathogens, bronchoalveolar lavage (BAL), transbronchial lung biopsy (TBLB), surgical lung biopsy (SLB), blood culture, urinary antigen test, and autopsy. Among the infectious disease cases, 25 cases were excluded because of the existence of co-infections. In addition, 11 cases which occurred within 4 weeks of the infection were excluded from this study because the HRCT findings of the current disease could have been influenced by the previous episode. Thus, 345 cases (199 males and 146 females; mean ± standard deviation, 56.2 ± 17.4 years; age range, 3–90 years) were included in this study. Some patients had multiple episodes; five patients had three episodes and 17 patients had two episodes. The final diagnoses in the 345 cases included were as follows: bacterial pneumonia ($n = 123$), PCP ($n = 105$), fungal infections ($n = 80$), TB ($n = 15$), CMV-P ($n = 11$), and septic embolism ($n = 11$). Diagnoses for these cases were established by detailed verification of the results of the sputum culture ($n = 105$), serum marker tests ($n = 97$ including β-D-glucan > 31 pg/mL [16], $n = 56$; *Aspergillus* antigen, $n = 30$; cryptococcal antigen, $n = 9$; *Candida* antigen, $n = 2$), BAL or TBLB ($n = 76$), blood culture ($n = 52$), SLB ($n = 3$), urinary antigen test ($n = 2$), and autopsy ($n = 10$). For PCP, elevation of the β-D-glucan level to more than 31 pg/mL is a good proven predictor [16]. All patients had underlying diseases (Table 1). To evaluate pulmonary complications, all patients underwent CT examinations within a few days of the onset of chest symptoms, including dyspnea and fever.

Computed tomography examination

The CT scans were acquired using the following systems: TCT-900S (Canon Medical Systems Corporation) (31 cases) and the Siemens Healthineers systems Somatom Plus 4 (70), Volume Zoom (71), Somatom Definition (70), and Somatom Sensation 64 (103). The CT scans were obtained at suspended end-inspiratory effort in the supine position without using any intravenous contrast material. After obtaining the 10-mm collimation scans at contiguous 10 mm intervals through the entire chest using the TCT-900S scanner, all patients underwent an HRCT through the region showing abnormal parenchymal findings at 2 mm collimation. After contiguous 10, 7, or 5 mm section imaging was performed through the chest using the other multislice CT scanners, additional HRCT images consisting of 1 or 2 mm collimated images were obtained at 1, 2, 5, or 10 mm intervals through the abnormal lung parenchyma. In all patients, the scanning parameters were 120 or 140 kVp and 160–250 effective mAs.

The image data were viewed on hard copy films during the scanning by the TCT-900S and were interfaced directly to our picture archiving and communication system (PACS) (ShadeQuest, Yokogawa Medical Solutions Corp.). The PACS displayed the image data on monitors (three monitors, 1280 × 1080 matrix, 8-bit viewable gray-scale) during the scanning by the other multislice CT scanners. The monitors were used to view both the lung (window width, 1500 or 1750 HU; window level, − 600 or − 700 HU) and mediastinal (window width, 250–400 HU; window level, 40–50 HU) window images.

Interpretation of the computed tomography images

The CT images were assessed independently in random order by two board-certified chest radiologists (15 and 28 years of experience, respectively) without any knowledge of the patients' clinical information except the immunocompromised state. Cases of discordant results between the two radiologists were resolved by consensus among them.

Each of the following HRCT findings were separately coded as "present" or "absent": (a) airspace consolidation; (b) GGA; (c) crazy-paving pattern; (d) mosaic pattern (mosaic perfusion); (e) nodules; (f) CT-halo sign; (g) tree-in-bud pattern; (h) bronchial wall thickening; (i) interlobular septal (ILS) thickening; (j) hilar or mediastinal lymph node (LN) enlargement; (k) pleural effusion. For HRCT findings (a), (b), (e), and the overall lesion, the extent of the lesions within the entire lung field was graded subjectively on a five-point scale (0 = 0%, 1 = 1–25%, 2 = 26–50%, 3 = 51–75%, and 4 = 76–100%).

The crazy-paving pattern was recorded as "present" if there was any superimposition of the interlobular or intralobular interstitial thickening within the GGA. The mosaic pattern was defined as sharply demarcated lung areas of inhomogeneous attenuation in which areas of the normal lung were seen intervening between the GGAs. When a mosaic pattern was present and it was difficult to differentiate infiltrative from airway diseases, we performed additional expiratory scanning (39 cases). The CT-halo sign was defined as a focal nodular opacity surrounded by the GGA. The tree-in-bud pattern was defined as a pattern in which small centrilobular nodules appeared connected to multiple branching, linear structures of a similar caliber and originating from the same stalk.

When a GGA or a consolidation was present, the predominance of the airspace consolidation or GGA (GGA/Cons predominance) was classified as GGA predominance, consolidation

Table 1 The characteristics and underlying diseases of patients with pulmonary infections

	Bacterial pneumonia (n=123)	PCP (n=105)	Fungal infection (n=80)	TB (n=15)	CMV-P (n=11)	Septic emboli (n=11)	*p*-value
Age, mean (SD)	55.8 (18.4)	58.2 (15.8)	54.8 (17.7)	61.7 (17.0)	51.7 (19.5)	50.0 (16.3)	0.333
Males, n (%)	78 (63.4)	49 (46.7)**	48 (60.0)	10 (66.7)	7 (63.6)	7 (63.6)	0.164
Underlying disease or condition, n (%)							<0.001
Hematologic malignancy without HSCT	37 (30.1)	29 (27.6)	20 (25.0)	2 (13.3)	3 (27.3)	6 (54.5)*	
Hematologic malignancy with HSCT	14 (11.4)	11 (10.5)	17 (21.3)*	1 (6.7)	4 (36.4)*	1 (9.1)	
Steroid or other immunosupressant	40 (32.5)**	56 (53.3)*	34 (42.5)	5 (33.3)	4 (36.4)	3 (27.3)	
Solid cancer with chemotherapy	25 (20.3)*	5 (4.8)**	8 (10.0)	3 (20.0)	0 (0)	1 (9.09)	
AIDS	0 (0)	4 (3.8)*	0 (0)	0 (0)	0 (0)	0 (0)	
Others	7 (1.7)	0 (0)**	1 (1.3)	4 (26.7)*	0 (0)	0 (0)	

PCP pneumocystis pneumonia, *CMV-P* cytomegalovirus pneumonia, *TB* tuberculosis, *HSCT* hematopoietic stem cell transplantation, *AIDS* acquired immunodeficiency syndrome

Others: chronic renal failure (n=4), chronic granulomatous diseases (n=1), and liver cirrhosis (n=1), chronic hepatitis (n=1), hypoalbuminemia (n=1) hypogammaglobulinemia (n=1), myocarditis (n=1), severe burns (n=1) and diabetes (n=1)

*Significantly higher (adjusted standard residuals >1.96) in groups

**Significantly lower (adjusted standard residuals <–1.96) in groups

predominance, or their equality. The distribution of GGA or airspace consolidation (GGA/Cons distribution) was classified as segmental, nonsegmental, or lobular. The nodules were classified according to their size as micro (< 3 mm), small (3–10 mm), or large (> 10 mm) and according to their distribution as centrilobular, perilymphatic, or random. Centrilobular distribution was defined as that in which the nodules were separated from the pleural surfaces, fissures, and interlobular septa by a distance of several millimeters. Perilymphatic distribution was defined as that in which the nodules were identified around the peribronchovascular interstitium, interlobular septa, and subpleural regions. Random distribution was defined as that in which the nodules did not show centrilobular or perilymphatic distribution and any specific distribution within the secondary pulmonary lobules.

Furthermore, the overall lesional distribution was classified axially (overall axial distribution) as central, peripheral, diffuse, or indeterminate and craniocaudally (overall craniocaudal distribution) as upper, lower, diffuse, or indeterminate.

Finally, one predominant CT pattern was recorded in each patient as follows: micro or small nodular pattern, large nodular pattern, diffuse GGA pattern, segmental GGA/Cons pattern, nonsegmental GGA/Cons pattern, and bronchial wall or ILS thickening pattern.

Statistical analysis

The mean age of the patients was calculated for each infection. The sex, underlying disease or condition of the patients, each CT finding, and CT pattern were compared among the infectious diseases using a chi-square (χ^2) test for independence. Age and the extent of the CT findings were compared using the Kruskal–Wallis test. Interobserver agreement between the two radiologists was calculated as the kappa value (κ) for the aforementioned HRCT findings from (a) to (k) and as intraclass correlation coefficient (ICC) for the extent of HRCT findings (a), (b), (e), and the overall lesion, and rated as follows: slight (0.00–0.20), fair (0.21–0.40), moderate (0.41–0.60), substantial (0.61–0.80), or almost perfect (0.81–1.00) [17]. We further defined the kappa value or ICC as high (more than 0.60, i.e., substantial to almost perfect) or low (less than 0.40, slight to fair). The extent of lesions was finalized as the average of grades allocated by two radiologists.

A p value less than 0.05 was considered as indicative of a significant difference. When the χ^2 test detected a significant difference among the groups, adjusted standardized residuals were calculated to identify the groups for which the CT findings contributed to the significant difference. An adjusted standardized residual of > 1.96 or <− 1.96 was considered indicative of a group with a significantly higher or lower frequency, respectively. In the next step, multiple logistic regression analyses were conducted in order to identify the significant indicator for the differentiation of each infectious disease from other infectious diseases, for example, between bacterial pneumonia and other infections (a combination of PCP, fungal infection, TB, CMV-P, and septic emboli). Forward selection (likelihood ratio) method was used for the multiple logistic regression analysis, and all variables including the parametric factors were included. The area under the curve (AUC) of each model was calculated. All statistical analyses were performed using SPSS software (version 22.0, IBM).

Table 2 The comparison of HRCT findings between pulmonary infections

		Bacterial pneumonia (n=123)	PCP (n=105)	Fungal infection (n=80)	TB (n=15)	CMV-P (n=11)	Septic emboli (n=11)	*p*-value	Agreement analysis
Consolidation, *n* (%)		104 (84.6)*	40 (38.1)**	45 (56.3)	11 (73.3)	8 (72.7)	6 (54.5)	<0.001	0.584
Cons-extent, mean (SD)		1.1 (0.6)	0.5 (0.6)	0.7 (0.6)	1.1 (0.7)	0.9 (0.5)	0.7 (0.6)	<0.001	0.652
GGA, *n* (%)		118 (95.9)	105 (100)*	63 (78.8)**	13 (86.7)	11 (100)	9 (81.8)	<0.001	0.502
GGA-extent, mean (SD)		1.5 (0.7)	3.1 (0.8)	1.1 (0.8)	1.3 (0.9)	2.5 (0.9)	1.0 (0.6)	<0.001	0.685
GGA-crazy-paving, *n* (%)		46 (37.4)	46 (43.8)*	18 (22.5)**	1 (6.7)**	7 (63.6)*	1 (9.1)	0.001	0.449
GGA-mosaic, *n* (%)		14 (11.4)**	69 (65.7)*	7 (8.8)**	3 (20.0)	4 (36.4)	0 (0)**	<0.001	0.533
GGA/Cons predominance, *n* (%)	Consolidation	56 (45.5)*	1 (1.0)**	25 (31.3)	8 (53.3)*	1 (9.1)	5 (45.5)	<0.001	0.545
	GGA	55 (44.7)**	104 (99.0)*	32 (40.0)**	4 (26.7)**	9 (81.8)	4 (36.4)		
	Equal	8 (6.5)	0 (0)**	7 (8.8)*	1 (6.7)	1 (9.1)	0 (0)		
GGA/Cons distribution, *n* (%)	Segmental	82 (66.7)*	3 (2.9)**	36 (45.0)*	9 (60.0)*	3 (27.3)	3 (27.3)	<0.001	0.280
	Non-segmental	14 (11.4)**	19 (18.1)	22 (27.5)*	1 (6.7)	4 (36.4)	6 (54.5)*		
	Lobular	23 (18.7)**	83 (79.0)*	6 (7.5)**	3 (20.0)	4 (36.4)	0 (0)**		
Nodule, *n* (%)		75 (61.0)	22 (21.0)**	64 (80.0)*	14 (93.3)*	6 (54.5)	11 (100)*	<0.001	0.522
Nodule-extent, mean (SD)		0.7 (0.7)	0.4 (0.7)	1.1 (0.7)	2.2 (1.1)	0.7 (0.6)	1.7 (1.0)	<0.001	0.635
Nodule size, *n* (%)	Micro	26 (21.1)*	4 (3.8)	8 (10.0)**	11 (73.3)*	1 (9.1)	1 (9.1)	<0.001	0.545
	Small	29 (23.6)	12 (11.4)	23 (28.8)	2 (13.3)	4 (36.4)	4 (36.4)		
	Large	20 (16.3)	6 (5.7)	33 (41.3)*	1 (6.7)**	1 (9.1)	6 (54.5)		
Nodules distribution, *n* (%)	Centrilobular	49 (39.8)*	10 (9.5)	23 (28.8)**	8 (53.3)	4 (36.4)	1 (9.1)**	0.002	0.578
	Perilymphatic	3 (2.4)	0 (0)	3 (3.8)	0 (0)	1 (9.1)	2 (18.2)*		
	Random	23 (18.7)**	12 (11.4)	38 (30.9)*	6 (40.0)	4 (36.4)	8 (72.7)		
Nodules with halo, *n* (%)		21 (17.1)	7 (6.7)**	28 (35.0)*	0 (0)	5 (45.5)*	6 (54.5)*	<0.001	0.476
Nodules with TIB, *n* (%)		28 (22.8)*	2 (1.9)**	10 (12.5)	6 (40.0)*	2 (18.2)	1 (9.1)	<0.001	0.390
Bronchial wall thickening, *n* (%)		80 (65.0)*	13 (12.4)**	36 (45.0)	8 (53.3)	2 (18.2)	7 (63.6)	<0.001	0.430
ILS thickening, *n* (%)		36 (29.3)	45 (42.9)*	13 (16.3)**	1 (6.7)**	5 (45.5)	3 (27.3)	<0.001	0.377
Axial Distribution, *n* (%)	Inner	7 (5.7)	4 (3.8)	1 (1.3)	0 (0)	1 (9.1)	0 (0)	<0.001	0.385
	Outer	40 (32.5)*	6 (5.7)**	31 (38.8)*	3 (20.0)	4 (36.4)	4 (36.4)		
	Diffuse	25 (20.3)**	82 (78.1)*	12 (15.0)**	7 (46.7)	5 (45.5)	3 (17.3)		
	Indeterminate	51 (41.5)*	13 (12.4)**	36 (45.0)*	5 (33.3)	1 (9.1)	4 (36.4)		
Craniocaudal Distribution, *n* (%)	Upper	22 (17.9)*	3 (2.9)**	9 (11.3)	3 (20.0)	0 (0)	2 (18.2)	<0.001	0.377
	Lower	48 (39.0)*	7 (6.7)**	26 (32.5)	1 (6.7)	3 (27.3)	4 (36.4)		
	Diffuse	15 (12.2)**	81 (65.9)*	13 (16.5)**	8 (53.3)	7 (63.6)	2 (18.2)		
	Indeterminate	38 (30.9)	14 (13.3)**	32 (40.0)*	3 (20.0)	1 (9.1)	3 (27.3)		
Overall extent, mean (SD)		2.1 (0.7)	3.3 (0.7)	1.8 (0.8)	2.8 (0.9)	2.8 (0.8)	2.1 (0.9)	<0.001	0.569
CT Pattern, *n* (%)	Small nodule	16 (13.0)	3 (2.9)**	18 (22.5)*	8 (53.3)*	1 (9.1)	5 (45.5)*	<0.001	0.493
	Large nodule	12 (9.8)	1 (1.0)**	25 (31.3)*	1 (6.7)	0 (0)	5 (45.5)*		
	Diffuse GGA	11 (8.9)**	85 (81.0)*	3 (3.8)**	2 (13.3)	7 (63.6)*	0 (0)**		

Table 2 (continued)

		Bacterial pneumonia (n=123)	PCP (n=105)	Fungal infection (n=80)	TB (n=15)	CMV-P (n=11)	Septic emboli (n=11)	*p*-value	Agreement analysis
	Segmental GGA/Cons	75 (61.0)*	3 (2.9)**	21 (26.3)	4 (26.7)	2 (18.2)	0 (0)**		
	Non-segmental GGA/Cons	8 (6.5)	13 (12.4)	12 (15.0)	0 (0)	1 (9.1)	1 (9.1)		
	Bronchial wall/ILS thickening	1 (0.5)	0 (0)	1 (1.3)	0 (0)	0 (0)	0 (0)		
LN swelling, n (%)		32 (26.0)	22 (21.0)	10 (12.5)**	3 (20.0)	1 (9.1)	5 (45.5)*	0.070	0.645
Effusion, n (%)		45 (36.6)	23 (21.9)**	26 (32.5)	5 (33.3)	5 (45.5)	8 (72.7)*	0.009	0.633

PCP pneumocystis pneumonia, *TB* tuberculosis, *CMV-P* cytomegalovirus pneumonia, *GGA* ground-glass attenuation, *Cons* consolidation, *TIB* tree-in-bud, *ILS* interlobular septum, *LN* lymph node

*Significantly higher (adjusted standard residuals >1.96) in groups

**Significantly lower (adjusted standard residuals <−1.96) in groups

Results

The patients' characteristics are shown in Table 1. There were no significant differences in age and sex ($p > 0.05$); however, there was a significant difference in the underlying diseases or condition ($p < 0.001$). Table 2 shows the comparison of HRCT findings between pulmonary infections. Interobserver agreement was fair to substantial (κ = 0.280–0.645 and ICC = 0.569–0.685). There were significant differences in almost all criteria ($p < 0.05$) except for LN enlargement ($p = 0.070$). Several HRCT findings were identified as the differentiating characteristics for each disease, after excluding the lower kappa values (< 0.40). For bacterial pneumonia, the predominance of consolidation (45.5%) was significantly frequent and the extent of consolidation was the largest (1.1). For PCP, the predominance of GGA (99.0%) and mosaic pattern (65.7%) were significantly frequent. The extent of GGA and overall lesion were the largest in PCP (3.1 and 3.3, respectively). For TB, the predominance of consolidation (53.3%) was significantly frequent and the extent of nodule was the largest (2.3). With respect to the predominant CT pattern in each infection, segmental GGA/Cons in bacterial pneumonia (61.0%), diffuse GGA in PCP (81.0%), nodules of small size (22.5%) and large size (31.3%) in fungal infections, nodules of small size (53.3%) in TB, diffuse GGA in CMV-P (63.6%), and nodules of small size (45.5%) and large size (45.5%) in septic embolism were significantly frequent.

Multiple logistic regression analyses identified 15 significant indicators, although positive predictive value (PPV) of some of those were relatively low (Tables 3 and 4).

For bacterial pneumonia (Fig. 1), the presence of bronchial wall thickening was an indicator ($p = 0.002$; odds ratio [OR], 2.341; 95% confidence interval [CI], 1.378–3.978) and sensitivity, specificity, PPV, and negative predictive value (NPV) were 65.0%, 70.3%, 54.8%, and 78.4%, respectively (Tables 3 and 4).

For PCP (Fig. 2), the presence of the mosaic pattern was an indicator ($p < 0.001$; OR, 9.808; 95% CI, 4.883–19.699) and sensitivity, specificity, PPV, and NPV were 65.7, 88.3, 71.1, and 85.5%, respectively. The absence of nodules was also a significant indicator ($p < 0.001$; OR, 6.834; 95% CI, 3.438–13.587) and sensitivity, specificity, PPV, and NPV were 79.0, 70.8, 54.2, and 88.5%, respectively (Tables 3 and 4).

For fungal infections (Fig. 3), the presence of nodules was an indicator ($p = 0.005$; OR, 2.531; 95% CI, 1.326–4.828) and sensitivity, specificity, PPV, and NPV were 80.0, 51.7, 33.3, and 89.5%, respectively (Tables 3 and 4).

The AUC of the model for PCP was the highest at 0.904. The AUC values for other infections were 0.697–0.763 (Table 3).

Table 3 The results of multiple logistic regression analysis

HRCT findings		Bacterial pneumonia (n=123)	Non-bacterial pneumonia (n=222)	Wald value	Odds Ratio [95% CI]	*p*-value	AUC
Consolidation	Positive	104 (84.6%)	110 (49.5%)	16.002	3.769 [1.967, 7.220]	<0.001	0.763
	Negative	19 (15.4%)	112 (50.5%)		……		
Mosaic pattern	Positive	14 (11.4%)	83 (37.4%)	13.969	……	<0.001	
	Negative	109 (88.6%)	139 (62.6%)		3.548 [1.826, 6.892]		
Bronchial wall thickening	Positive	80 (65.0%)	66 (29.7%)	9.888	2.341 [1.378, 3.978]	0.002	
	Negative	43 (35.0%)	156 (70.3%)		……		
HRCT findings		PCP (n=105)	Non-PCP (n=240)	Wald value	Odds Ratio [95% CI]	*p*-value	AUC
Mosaic pattern	Positive	69 (65.7%)	28 (11.7%)	41.180	9.808 [4.883, 19.699]	<0.001	0.904
	Negative	36 (34.3%)	212 (88.3%)		……		
Nodule	Positive	22 (21.0%)	170 (70.8%)	30.050	……	<0.001	
	Negative	83 (79.0%)	70 (29.2%)		6.834 [3.438, 13.587]		
Bronchial wall thickening	Positive	13 (12.4%)	133 (55.4%)	11.703	……	0.001	
	Negative	92 (87.6%)	107 (44.6%)		3.859 [1.780, 8.364]		
Consolidation	Positive	40 (38.1%)	174 (72.5%)	10.067	……	0.002	
	Negative	65 (61.9%)	66 (27.5%)		3.193 [1.559, 6.541]		
Pleural effusion	Positive	23 (21.9%)	89 (34.9%)	4.792	……	0.029	
	Negative	82 (78.1%)	151 (62.9%)		2.393 [1.096, 5.227]		
HRCT findings		Fungal infection (n=80)	Non-fungal infection (n=265)	Wald value	Odds Ratio [95% CI]	*p*-value	AUC
Nodule	Positive	64 (80.0%)	128 (48.3%)	7.934	2.531 [1.326, 4.828]	0.005	0.721
	Negative	16 (20.0%)	137 (51.7%)		……		
GGA	Positive	63 (78.8%)	256 (96.6%)	10.265	……	0.001	
	Negative	17 (21.3%)	9 (3.4%)		4.213 [1.748, 10.154]		
Mosaic pattern	Positive	7 (8.8%))	90 (34.0%)	6.597	……	0.010	
	Negative	73 (91.3%)	175 (66.0%)		3.090 [1.306, 7.309]		
HRCT findings		TB (n=15)	Non-TB (n=330)	Wald value	Odds Ratio [95% CI]	*p*-value	AUC
Nodule	Positive	14 (93.3%)	178 (53.9%)	5.681	11.955 [1.554, 91.967]	0.017	0.697
	Negative	1 (6.7%)	152 (46.1%)		……		
HRCT findings		CMV-P (n=11)	Non-CMV-P (n=334)	Wald value	Odds Ratio [95% CI]	*p*-value	AUC
Crazy-paving	Positive	7 (63.6%)	112 (33.5%)	5.031	4.372 [1.205, 15.868]	0.025	0.718
	Negative	4 (36.4%)	222 (66.5%)		……		
Nodules with halo	Positive	5 (45.5%)	62 (18.6%)	5.808	4.720 [1.336, 16.677]	0.016	
	Negative	6 (54.5%)	272 (81.4%)		……		
HRCT findings		Septic emboli (n=11)	Non-Septic emboli (n=334)	Wald value	Odds Ratio [95% CI]	*p*-value	AUC
Pleural effusion	Positive	8 (72.7%)	104 (31.1%)	6.667	5.897 [1.534, 22.680]	0.010	0.708
	Negative	3 (27.3%)	230 (68.9%)		……		

PCP pneumocystis pneumonia, *CMV-P* cytomegalovirus pneumonia, *GGA* ground-glass attenuation, *LN* lymph node, *CI* confidence interval, *AUC* area under the curve

Table 4 Sensitivity, specificity, accuracy, PPV, and NPV of each HRCT finding for detecting each infection

	Sensitivity	Specificity	Accuracy	PPV	NPV
Bacterial pneumonia					
Presence of consolidation	84.6%	50.5%	62.6%	48.6%	85.5%
Presence of bronchial wall thickening	65.0%	70.3%	68.4%	54.8%	78.4%
Absence of mosaic pattern	88.6%	37.4%	55.7%	44.0%	85.6%
PCP					
Presence of mosaic pattern	65.7%	88.3%	81.4%	71.1%	85.5%
Absence of nodules	79.0%	70.8%	73.3%	54.2%	88.5%
Absence of bronchial wall thickening	87.6%	55.4%	65.2%	46.2%	91.1%
Absence of consolidation	61.9%	72.5%	69.3%	49.6%	81.3%
Absence of pleural effusion	78.1%	34.9%	49.6%	35.2%	79.5%
Fungal infection					
Presence of nodules	80.0%	51.7%	58.3%	33.3%	89.5%
Absence of GGA	21.3%	96.6%	79.1%	65.4%	80.3%
Absence of mosaic pattern	91.3%	34.0%	47.2%	29.4%	92.8%
TB					
Presence of nodules	93.3%	46.1%	48.1%	7.3%	99.3%
CMV-P					
Presence of crazy-paving	63.6%	66.5%	66.4%	5.9%	98.2%
Presence of nodules with halo	45.5%	81.4%	80.3%	7.5%	97.8%
Septic embolism					
Presence of pleural effusion	72.7%	68.9%	69.0%	7.1%	98.7%

PPV positive predictive value, *NPV* negative predictive value, *PCP* pneumocystis pneumonia, *TB* tuberculosis, *CMV-P* cytomegalovirus pneumonia, *GGA* ground-glass attenuation, *Cons* consolidation, *TIB* tree-in-bud, *ILS* interlobular septum, *LN* lymph node

Discussion

Our study showed that segmental GGA/Cons in bacterial pneumonia, diffuse GGA in PCP and CMV-P, and nodules in fungal infections, TB, and septic embolism were the significantly frequent CT patterns in immunocompromised patients.

It is difficult to accurately evaluate the HRCT findings of pulmonary infections in immunocompromised patients because of the nonspecific or atypical imaging patterns. However, our study suggested that the differentiation between the various pulmonary infections in immunocompromised patients might be partially possible by evaluating several HRCT findings.

Furthermore, the present study identified three significant indicators, using the multiple logistic regression analyses, which may be useful for differentiating various pulmonary infections.

Our multiple logistic regression analyses suggested that bronchial wall thickening may serve as a potential indicator for bacterial pneumonia, and the same is true for the presence of consolidation despite the relatively low PPV of this indicator (48.6%). Several studies on immunocompetent patients reported that GGA (79.4–90.8%), bronchial wall thickening (60.3–85.8%), centrilobular nodules (47.1–72.5%), and consolidation (48.6–58.6%) are common characteristics of bacterial pneumonia [18–20]. *Pseudomonas aeruginosa* and *S. aureus* infections tend to show a bronchopneumonia pattern, while *Streptococcus pneumoniae* and *Klebsiella pneumoniae* infections show a lobar pneumonia pattern [15, 21]. A review of HRCT findings for 114 patients (58 immunocompetent and 59 immunocompromised) showed that consolidation was not detected in viral pneumonia, and was more frequently observed in bacterial pneumonia (85%) than in PCP (9%) [22]. Segmental consolidation is frequent in community-acquired bacterial pneumonia [23]. Though immunocompromised patients may show atypical findings, our study revealed HRCT findings for bacterial pneumonia in immunocompromised patients similar to those reported for immunocompetent patients.

Patients with PCP frequently exhibit the mosaic pattern, and nodules with or without cavitation are infrequent [24–26]. Nodules and cystic lesions are relatively common in acquired immunodeficiency syndrome (AIDS) patients [24]. The HRCT findings of PCP and CMV-P are often similar, but the differential diagnosis of these is typified by a mosaic pattern and an apical distribution in PCP and an ill-defined demarcation of GGA, consolidation, and nodules with or without a halo sign in CMV-P [27, 28]. These findings of

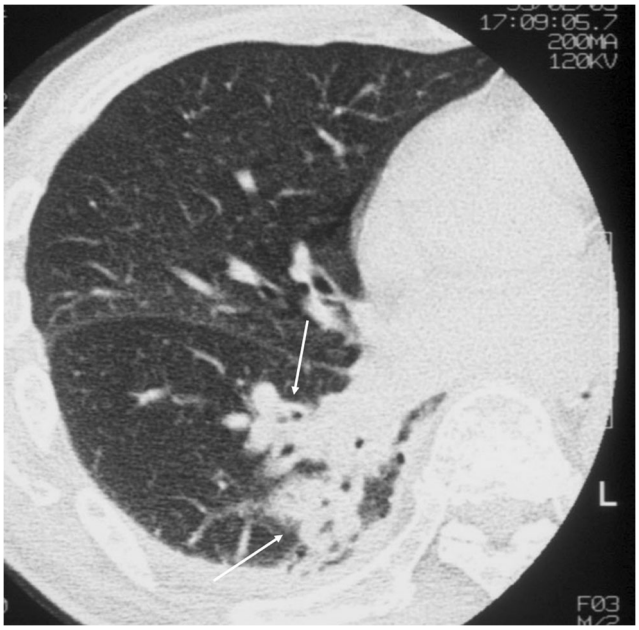

Fig. 1 Bacterial pneumonia in a 64-year-old man with multiple myeloma. High-resolution computed tomography shows thickening of the bronchial wall (arrows)

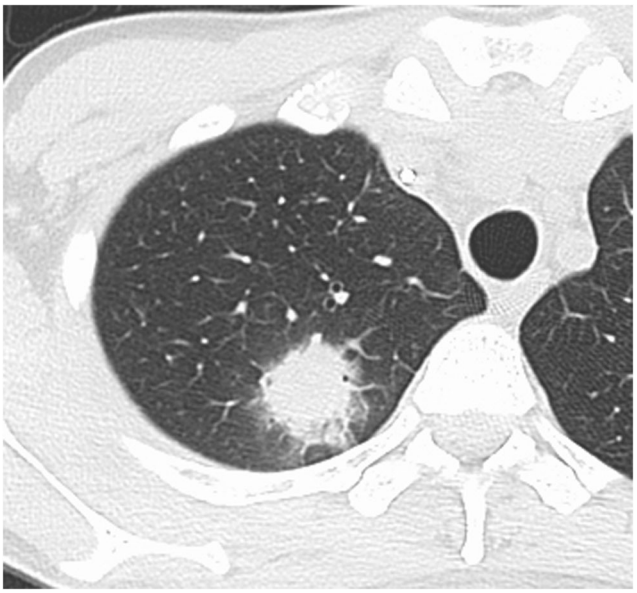

Fig. 3 Invasive aspergillosis in a 27-year-old man with chronic myeloid leukemia. High-resolution computed tomography shows a large nodule with a halo sign

these reports support our results, which identified the presence of a mosaic pattern and the absence of nodules as potential indicators for PCP. We identified the presence of nodules with a halo sign as an indicator for CMV-P, albeit with very low PPV (7.5%).

Our study showed that the presence of nodules could be an indicator for fungal infection. In invasive aspergillosis in immunocompromised patients, nodules with the halo sign in the early phase, and cavitary lesions in the late phase, are common [29, 30]. Nodules and cavitation are common findings in cryptococcosis [31], and nodules with centrilobular or random distribution are common in candidiasis [15, 32].

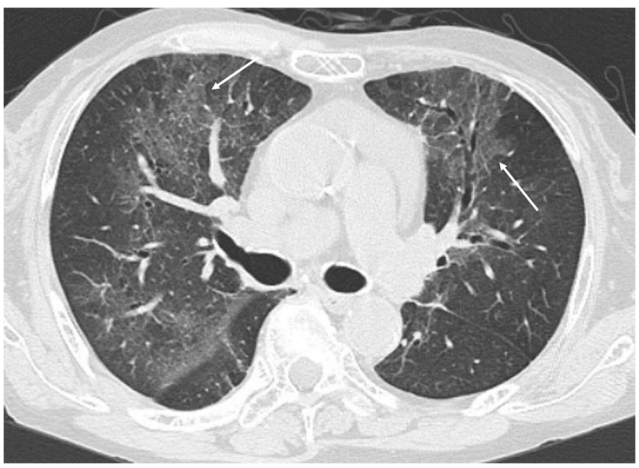

Fig. 2 Pneumocystis pneumonia in a 70-year-old woman with pericarditis under steroid therapy. High-resolution computed tomography shows bilateral ground-glass attenuation with a mosaic pattern (arrows) and reticulation

Nodules, tree-in-bud appearance, consolidation, and cavities in the upper lobe are the most common findings observed in TB, but immunocompromised patients show more atypical findings, such as multiple cavities and lower or nonsegmental distribution [33, 34]. Our study identified the presence of nodule as highly suggestive of TB, albeit with very low PPV (7.3%). We found nodules to be the predominant patterns for septic embolism, with pleural effusion identified as an indicator with very low PPV (7.1%).

In our study, the AUC of the model for PCP was the highest (0.904), but the AUC values for other infections were lower (0.697–0.763) than that for PCP.

Our study had several limitations. First, this study was retrospective in nature; therefore, the CT protocols and diagnostic procedures for the included subjects were diverse. Second, the systematic and generalized evaluation of CMV-P, TB, and septic embolism was limited to a relatively small number of patients compared to that of bacterial pneumonia, fungal infections, and PCP. Third, the reliability of the diagnosis may be controversial in patients without a pathologic confirmation of the disease. However, patients with infections due to other organisms or other lung diseases, which might have confounded evaluation of their HRCT findings, were excluded from our study, and diagnoses within our study population were strongly supported by serum markers or urinary antigen tests. Fourth, we report high overall interobserver variability in the determination of GGA/Cons distribution and of axial and craniocaudal lesion distribution. These criteria were not simple binary variables. Therefore, interindividual variations may be noted in the reading of such multiple categorical findings by board-

certified chest radiologist, which should be taken into account during differential diagnosis.

In conclusion, HRCT could be used for the differential diagnosis of pulmonary infections in immunocompromised patients.

Funding The authors state that this work has not received any funding.

Compliance with ethical standards

Guarantor The scientific guarantor of this publication is Nobuyuki Tanaka.

Conflict of interest The authors declare that they have no conflict of interest.

Statistics and biometry One of the authors, Reo Kawano, has significant statistical expertise and provided statistical advice for this manuscript.

Informed consent Written informed consent was waived by the Institutional Review Board because this study was a retrospective study.

Ethical approval Institutional Review Board approval was obtained.

Methodology
- retrospective
- case–control study
- performed at one institution

References

1. Yildiz O, Doganay M (2006) Actinomycoses and Nocardia pulmonary infections. Curr Opin Pulm Med 12(3):228–234
2. Thomas CF Jr, Limper AH (2004) Pneumocystis pneumonia. N Engl J Med 350:2487–2498
3. Boeckh M, Geballe AP (2011) Cytomegalovirus: pathogen, paradigm, and puzzle. J Clin Invest 121(5):1673–1680
4. Franquet T (2006) High-resolution computed tomography (HRCT) of lung infections in non-AIDS immunocompromised patients. Eur Radiol 16:707–718
5. Cook RJ, Ashton RW, Aughenbaugh GL et al (2005) Chest 128(1): 162–166
6. Jorens PG, Van Marck E, Snoeckx A, Parizel PM (2009) Nonthrombotic pulmonary embolism. Eur Respir J 34(2):452–474
7. Bach AG, Restrepo CS, Abbas J et al (2013) Imaging of nonthrombotic pulmonary embolism: biological materials, nonbiological materials, and foreign bodies. Eur J Radiol 82(3):e120–e141
8. Primack SL, Müller NL (1994) High-resolution computed tomography in acute diffuse lung disease in the immunocompromised patients. Radiol Clin North Am 32:731–744
9. Worthy S, Kang EY, Müller NL (1995) Acute lung disease in the immunocompromised host: differential diagnosis at high-resolution CT. Semin Ultrasound CT MRI 16:353–360
10. Oh YW, Effmann EL, Godwin JD (2000) Pulmonary infections in immunocompromised hosts: the importance of correlating the conventional radiologic appearance with the clinical setting. Radiology 217:647–656
11. Heussel CP, Kauczor HU, Heussel G, Fischer B, Mildenberger P, Thelen M (1997) Early detection of pneumonia in febrile neutropenic patients: use of thin-section CT. AJR Am J Roentgenol 169: 1347–1353
12. Kim HJ, Park SY, Lee HY, Lee KS, Shin KE, Moon JW (2014) Ultra-low-dose chest CT in patients with neutropenic fever and hematologic malignancy: image quality and its diagnostic performance. Cancer Res Treat 46:393–402
13. Worthy SA, Flint JD, Müller NL (1997) Pulmonary complications after bone marrow transplantation: high resolution CT and pathologic findings. Radiographics 17:1359–1371
14. Brown MJ, Miller RR, Müller NL (1994) Acute lung disease in the immunocompromised host: CT and pathologic examination findings. Radiology 190:247–254
15. Tanaka N, Kunihiro Y, Yanagawa N (2018) Infection in immunocompromised hosts: imaging. J Thorac Imaging 33(5):306–321
16. Tasaka S, Hasegawa N, Kobayashi S et al (2007) Serum indicators for the diagnosis of pneumocystis pneumonia. Chest 131:1173–1180
17. Kundel HL, Polansky M (2003) Measurement of observer agreement. Radiology 228(2):303–308
18. Okada F, Ando Y, Tanoue S et al (2012) Radiological findings in acute Haemophilus influenzae pulmonary infection. Br J Radiol 85(1010):121–126
19. Morikawa K, Okada F, Ando Y et al (2012) Meticillin-resistant Staphylococcus aureus and meticillin-susceptible S. aureus pneumonia: comparison of clinical and thin-section CT findings. Br J Radiol 85(1014):e168–e175
20. Okada F, Ando Y, Nakayama T et al (2011) Pulmonary thin-section CT findings in acute Moraxella catarrhalis pulmonary infection. Br J Radiol 84(1008):1109–1114
21. Reynolds JH, McDonald G, Alton H, Gordon SB (2010) Pneumonia in the immunocompetent patient. Br J Radiol 83(996):998–1009
22. Reittner P, Ward S, Heyneman L, Johkoh T, Müller NL (2003) Pneumonia: high-resolution CT findings in 114 patients. Eur Radiol 13(3):515–521
23. Tanaka N, Matsumoto T, Kuramitsu T et al (1996) High resolution CT findings in community-acquired pneumonia. J Comput Assist Tomogr 20(4):600–608
24. Boiselle PM, Crans CA Jr, Kaplan MA (1999) The changing face of Pneumocystis carinii pneumonia in AIDS patients. AJR Am J Roentgenol 172:1301–1309
25. Kuhlman JE, Kavuru M, Fishman EK et al (1990) Pneumocystis carinii pneumonia: spectrum of parenchymal CT findings. Radiology 175:711–714
26. Fujii T, Nakamura T, Iwamoto A (2007) Pneumocystis pneumonia in patients with HIV infection: clinical manifestations, laboratory findings, and radiological features. J Infect Chemother 13(1):1–7
27. Vogel MN, Brodoefel H, Hierl T et al (2007) Differences and similarities of cytomegalovirus and pneumocystis pneumonia in HIV-negative immunocompromised patients thin section CT morphology in the early phase of the disease. Br J Radiol 80(955):516–523
28. Kunihiro Y, Tanaka N, Matsumoto T, Yamamoto N, Matsunaga N (2015) The usefulness of a diagnostic method combining high-resolution CT findings and serum markers for cytomegalovirus pneumonia and pneumocystis pneumonia in non-AIDS patients. Acta Radiol 56(7):806–813
29. Kuhlman JE, Fishman EK, Burch PA, Karp JE, Zerhouni EA, Siegelman SS (1987) Invasive pulmonary aspergillosis in acute leukemia. The contribution of CT to early diagnosis and aggressive management. Chest 92(1):95–99
30. Brodoefel H, Vogel M, Hebart H et al (2006) Long-term CT follow-up in 40 non-HIV immunocompromised patients with invasive pulmonary aspergillosis: kinetics of CT morphology and correlation

with clinical findings and outcome. AJR Am J Roentgenol 187(2): 404–413
31. Chang WC, Tzao C, Hsu HH et al (2006) Pulmonary cryptococcosis: comparison of clinical and radiographic characteristics in immunocompetent and immunocompromised patients. Pulmonary cryptococcosis: comparison of clinical and radiographic characteristics in immunocompetent and immunocompromised patients. Chest 129(2):333–340
32. Franquet T, Müller NL, Lee KS, Oikonomou A, Flint JD (2005) Pulmonary candidiasis after hematopoietic stem cell transplantation: thin-section CT findings. Radiology 236(1):332–337
33. Ikezoe J, Takeuchi N, Johkoh T et al (1992) CT appearance of pulmonary tuberculosis in diabetic and immunocompromised patients: comparison with patients who had no underlying disease. AJR Am J Roentgenol 159(6):1175–1179
34. Mathur M, Badhan RK, Kumari S, Kaur N, Gupta S (2017) Radiological manifestations of pulmonary tuberculosis—a comparative study between immunocompromised and immunocompetent patients. J Clin Diagn Res 11(9):TC06–TC09